EVS30 Symposium
Stuttgart, Germany, October 9 - 11, 2017

Iron Loss Modelling of a PMSM Traction Motor, Including Magnetic Degradation due to Lamination Laser Cutting

Lode Vandenbossche[1], Sven Luthardt[2], Sigrid Jacobs[3], Stefan Schmitz[2], Axel Heitmann[2]
Emmanuel Attrazic[4]

[1]*ArcelorMittal Global R&D Gent, OCAS, Pres. J. F. Kennedylaan 3, B-9060 Zelzate, Belgium*

[2]*Porsche AG, Entwicklung Antrieb, Porschestraße 911, D-71287 Weissach, Germany*

[3]*(corresp. author) ArcelorMittal Global R&D, Technologiepark 935, B-9052 Zwijnaarde (Gent), Belgium, sigrid.jacobs@arcelormittal.com*

[4]*ArcelorMittal Saint-Chély d'Apcher, Rue des Martyrs du Maquis, F-48200 Saint-Chély d'Apcher, France*

Summary

To narrow down the existing gap between ordinary calculated and actually measured iron losses in electrical machines, one of the possible improvements is to incorporate the local magnetic degradation due to lamination cutting, into the modelling of the electrical steel parts of the machine. In this paper such improved calculation is applied and validated on a laser cut prototype of a permanent magnet synchronous traction motor for a battery electric vehicle, using an ArcelorMittal iCARe® electrical steel grade developed for automotive traction. The additional iron losses due to laser cutting are significant, are of both hysteretic and excess loss origin, and strongly depend on the machine's operational point. Such improved machine modelling that incorporates the cutting effect enhances the predictive power of the machine loss modelling and hence enables more accurate optimisation of the motor design.

Keywords: Motor design, permanent magnet motor, efficiency, materials, battery electric vehicle.

1 Introduction

Manufacturing processes to produce electrical machines have an impact on the actual machine performance: processes such as punching or laser cutting of electrical steel laminations lead to a local degradation of the magnetic steel characteristics near the cut edges, which in turn deteriorate the performance and efficiency of the electrical machine.

During the design stage of the machine, ordinary machine modelling based on unaffected homogeneous magnetic properties of electrical steels such as standard Epstein data, typically leads to a significant under-estimation of the iron losses occurring in the actually manufactured machines. However when aiming to effectively optimize the machine design, such uncertainties in the loss prediction should be reduced significantly, for instance by taking into account the effect of cutting on the local magnetic properties and hence on the machine performance.

Indeed, when aiming to improve the calculation accuracy of the electrical machine's efficiency map, for the machine designer it is necessary to understand, to quantify and to be able to incorporate into the machine modelling the influence of manufacturing processes, which includes the cutting of the electrical steel parts. Such enhanced modelling approach leads to a better forecast of the continuous power during the design stage and avoids the over-engineering of the electrical machine with respect to the vehicle requirements. Furthermore, when including the effect of cutting into the electrical machine modelling, a more realistic comparison of different machine topologies and geometries can be carried out during the design stage.

In this paper, such methodology is applied and validated on a permanent magnet synchronous traction motor (PMSM) for a battery electric vehicle. This study includes numerical simulations (finite element analysis of the machine, combined with iron loss post-processing), and experimental work (both advanced material characterization, as well as machine performance measurements on the prototype traction motor).

The electrical machine used in this investigation is an interior permanent magnet synchronous machine, which offers a high power density for traction application. The main parameter specifications of this particular traction machine are listed in Table 1.

The machine's maximum speed (15000 rpm) corresponds with a fundamental electrical frequency of 1 kHz. Hence for this particular application a dedicated thin low loss fully processed electrical steel grade, optimized for lowest iron losses in the medium frequency range (400 – 1000 Hz), is chosen from the iCARe® range of electrical steels, which are developed specifically for automotive traction applications operating at such frequencies.

Table 1: Parameter specifications, of the PMSM machine under investigation

Machine parameter	Specification
Rotor topology	Interior V-shaped 3 layers
Permanent magnet material	NdFeB
Number of poles	8
Number of stator slots	72
Winding topology	Distributed winding
Outer diameter	180 mm
Axial length	185 mm
Maximum speed	15000 rpm
Nominal DC-voltage	800 V
Cooling	Water-jacket cooled

2 Losses in permanent magnet synchronous machines

The losses occurring in permanent magnet synchronous machines have different origins and consist of iron losses, permanent magnet losses, copper losses, bearing losses and air friction losses:

- The copper conductor or Joule losses can be calculated based on the stator current measurement, once the stator winding resistance is properly determined;
- The bearing losses can be determined with a no-load test setup, or by analytical calculations based on technical data provided by the bearing manufacturer;
- The air friction losses can be determined by CFD simulations, or can be based on experiments;
- For interior permanent magnet arrangements, the permanent magnet losses are much lower than the iron losses under sinusoidal current excitation [1];
- The iron losses occur in the stator and the rotor laminations of the machine. The stator iron losses are typically more significant than the rotor iron losses, but the rotor iron losses are thermally more critical for the continuous power of the motor. In the next section, the approach to compute the iron losses is described in more detail.

3 Iron loss modelling approach

The iron loss modelling methodology for rotating electrical machines can be enhanced by taking into account the interplay between the machine's operational aspects (such as rotational flux and higher harmonics) and the machine's manufacturing aspects (such as lamination cutting). Such modelling approach can be seen as a further elaborated Bertotti-based iron loss separation model [2-4], but is also taking into account the lamination cutting effect on the local magnetization curve *J(H,x)*, as well as on the local iron loss parameters $s_{hyst}(x)$, $s_{exc}(x)$, $\alpha(x)$ and $\gamma(x)$ of the electrical steel under test, as a function of distance from the cut edge *x*:

$$P(x, J(x), f_0) = P_{hyst} + P_{eddy} + P_{exc} = s_{hyst}(x)\left(1+(r-1)\cdot\frac{J_{\min}(x)}{J_p(x)}\right)J_p(x)^{\alpha(x)} f_0 + s_{eddy}\sum_{n=1}^{\infty}(J_{p,n}(x))^2(nf_0)^2 + s_{exc}(x)\sum_{n=1}^{\infty}(J_{p,n}(x))^{\gamma(x)}(nf_0)^{1.5} \quad (1)$$

Experimental methodologies were developed [5-6] which are capable to determine both local magnetic properties as continuous functions of *x*. For the finite element computations however, it is more convenient and pragmatic to divide the stator and rotor into different zones, with for each zone different allocated material properties, especially in case of laser cutting, as explained later in section 4.

The main objective of this study reported in this paper is to evaluate how the degradation of the electrical steel's magnetic properties influences the machine's global iron losses, its efficiency and performance, for a PMSM traction motor for a battery electric car. Therefore two iron loss calculations are carried out in parallel, in order to evaluate the gain in accuracy when including the cut edge effect:

(a) **Unaffected case** (ordinary model) based on homogeneous and unaffected material properties;
(b) **Affected case** including the magnetic degradation due to laser cutting (enhanced model).

Furthermore, the iron loss modelling results when including the laser cutting effect are validated by machine measurements on a laser cut prototype machine.

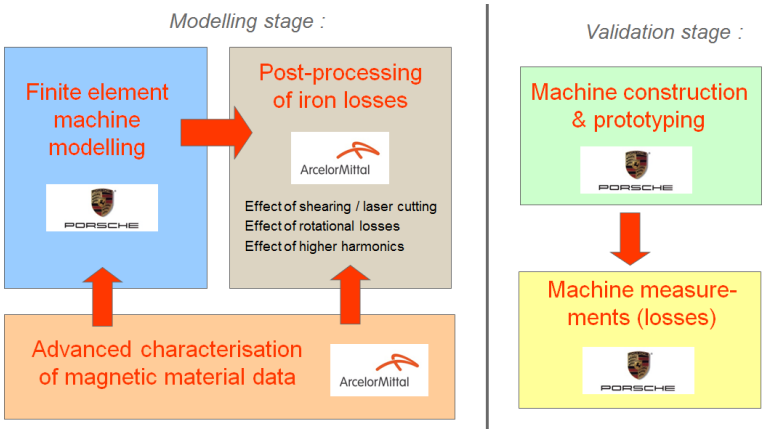

Figure 1: Schematic overview of the iron loss modelling project, and its validation on a prototype machine.

Fig. 1 shows the followed methodology overview. The modelling stage consists of three main parts:

(1) ***Advanced material characterisation***, serving as input for the other two tasks. These local magnetic properties describing the degradation near the cut edge are determined by a dedicated experimental procedure on strips cut to different widths (see section 4 for more details).

(2) ***Finite element computation*** of the magnetic flux density distribution in the electrical steel parts. The machine operation is simulated by a 2D time-stepping Finite-Element technique, with the geometry divided into several zones, each having its own magnetisation curve and loss parameters (as determined in part 1).

(3) ***Iron loss calculation via post-processing routines***: the local magnetic flux densities extracted from the finite element calculation (part 2) as well as the local loss parameters (determined in part 1) are post-processed into the computed iron losses by considering phenomena such as higher harmonics, rotational losses as well as the degradation by cutting.

4 Characterisation of the laser cutting effect on the magnetic properties

Laser cutting has a significant detrimental impact on the magnetic properties of the cut electrical steel components: compared to the unaffected material, the permeability and remanence decrease, whereas the coercivity and iron losses increase. Laser cutting induces thermal stresses due to the occurrence of high temperature gradients within the material during the cutting process, and the magnetisation processes are influenced by the remaining residual stress distribution after this thermal process is finished. The zone within which the magnetic properties are affected appears to be fairly large, in literature degradation depths due to laser cutting of 15 to 20mm are reported [8-9]. In comparison, the magnetic degradation depth due to punching is around of 5 to 7mm [5-6][9], so roughly three times smaller. Moreover, through cutting by laser, the decrease of the local magnetic flux is observed over the total width of the strip (in [9], strips up to 30mm in width were investigated), so not only at the cut edges as is the case for punching.

In order to characterize the laser cutting effect on the magnetic properties, rectangular strips of different widths (between 5 and 60 mm) were laser cut, both along the rolling (RD) and transversal direction (TD). These strips are laser cut out of the same production batch of the electrical steel that is utilised to manufacture the prototype PMSM machine under investigation in this paper. Moreover, the same laser cutting device and processing parameters were used as for the cutting of the stator and rotor laminations, in order to make the magnetic properties of the strips as representative as possible to the laser cut affected magnetic properties of the electrical steel parts of the prototype electrical machine.

All geometrical details of the stator and rotor laminations of the PMSM under test are significantly smaller than 10mm, which means that they are also significantly smaller than the depth of the laser cut degraded zone (as said before, in literature values of around 15 to 20mm are found [8-9]). Hence it was decided to directly utilise the measured magnetic properties obtained on laser cut strips having a width as close as possible to the geometrical details of the stator and rotor parts, into the laser cut affected model.

More specifically, for the laser cut affected model, the stator is divided into two regions: stator yoke and stator teeth, and the strip widths closest to the stator yoke and stator teeth width are found to be 10mm and 5mm respectively. Dealing with the rotor having an interior permanent magnet topology, the strips of 5mm width are closest to the rotor geometrical details. As a summary, the measured magnetic properties obtained on the laser cut strips of 10mm wide are used as input for the stator yoke region, whereas the measured magnetic properties obtained on the laser cut strips of 5mm represent both the stator teeth region and rotor region of the particular machine geometry under investigation.

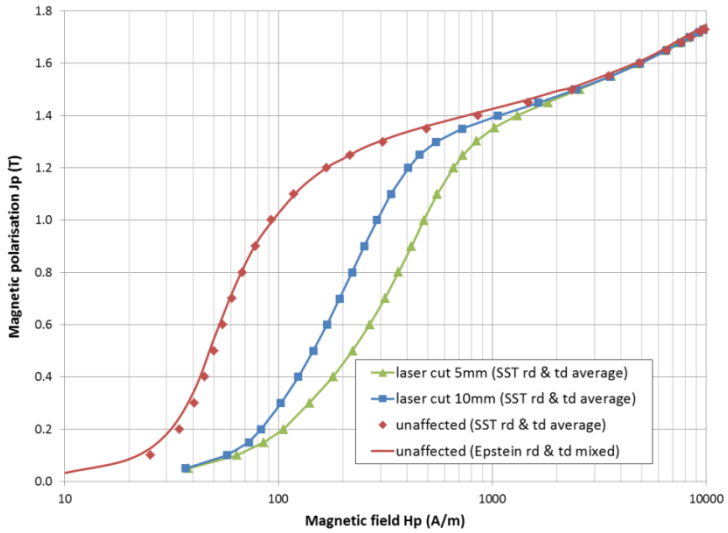

Figure 2: Measured magnetisation curves at 50Hz, on the laser cut affected strips of 5mm and 10mm wide, as well as on the unaffected (sheared) Epstein strips.

The magnetic characterisations on the laser cut strips are carried out using a single sheet tester (SST). To average out any possible variability of the laser cut effect, always a total width of 60mm is placed inside the SST. In other words, 6 strips of 10mm wide (or 12 strips of 5mm wide) are placed next to each other to be measured together at the same time. Two such sample sets of equal individual widths, one along RD and one along TD, are measured separately and the obtained magnetic properties along RD and TD are then averaged to be more representative for the magnetic properties along any direction occurring in the rotating machine application. The magnetic path length of the utilised SST is correlated to the Epstein frame.

On the other hand, to build up the unaffected material model, strips of 30mm wide are cut by guillotine shearing, again along both RD and TD, as is the common practice to prepare strips for Epstein frame testing. These guillotine sheared strips represent the unaffected material and are also characterised with the SST in an identical way as the laser cut strips, meaning that two 30mm wide strips are measured at once, and RD and TD properties are averaged out afterwards.

Fig. 2 shows the magnetisation curves measured on both ‘affected’ laser cut strip sets of 10mm and 5mm wide, as well as the one measured on the ‘unaffected’ 30mm wide sheared strips. To validate the SST-to-Epstein correlation of the magnetic path length of the SST, also the magnetisation curve measured on the same 30mm wide sheared strips, but now mounted inside the Epstein frame is shown in Fig. 2, which shows a good correspondence to the SST measurement on the same strips.

The effect of laser cutting on the magnetisation curve as shown in Fig. 2 appears to be significant: around the knee of the magnetisation curve the magnetic permeability of the laser cut 5mm wide strip is up to five times lower than for the unaffected material (for the unaffected material, 1T is reached when applying 100 A/m, whereas for the laser cut 5mm wide strip, 500 A/m applied magnetic field is necessary to obtain 1T).

On the same sample sets, and with the same SST methodology, also the iron losses are measured for a frequency range from 50 Hz to 1 kHz and for a polarisation range from 0.1 T till 1.8 T. These iron losses are then used to determine the parameters of the iron loss description as given in Equation (1). Fig. 3 shows the relative change of the iron loss parameters of the concerned laser cut strip widths 5mm and 10mm, when compared to the iron loss parameters of the unaffected material. The parameters of those loss components that are known to be dependent on changes of microstructure and/or (residual) mechanical stresses, being both the hysteresis and the excess losses, are significantly influenced by the laser cutting.

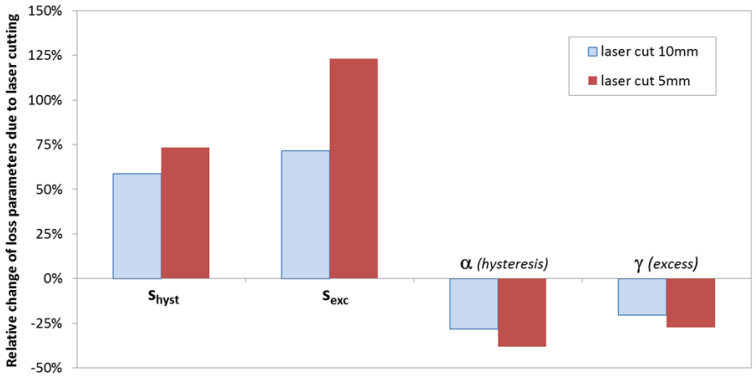

Figure 3: Relative change of the iron loss parameters due to laser cutting, compared to the unaffected properties, measured on the sheared Epstein strips.

5 Results of the machine modelling

5.1 Calculated torque results

Machine calculations are carried out by finite element analysis for no load conditions, as well as at 70 load operational points (15 different speeds, combined with – depending on the speed – 3 to 6 load conditions). Each of these operational points is defined by a certain stator current input, which is identical for both unaffected and laser cut affected models.

For each of these operational points, the machine calculations are carried out twice, firstly with the unaffected magnetisation curve (see Fig. 2) as input for all electrical steel parts of the machine, and secondly with the laser cut affected magnetisation curves: as discussed before in section 4, the magnetisation curve measured on the laser cut strips of 10mm wide are used as input for the stator yoke region, whereas the magnetisation curve obtained on the laser cut strips of 5mm represents both the stator teeth region and rotor region of the machine's geometry.

The calculated torque for six different load operational points within the non-flux-weakened (constant torque) region of the speed-torque operational plane (meaning for speeds less or equal than 6000 rpm) is compared in Table 2, for both affected and unaffected models.

Table 2: Comparison of the calculated torque, for six different non-flux-weakened operational points

Operational Point	Calculated torque (Nm); unaffected material model	Calculated torque (Nm); affected model (laser cutting)	Difference (%)
load-1	4.87	4.83	-0.8%
load-2	60.3	59.8	-0.8%
load-3	120.8	119.8	-0.8%
load-4	181.6	180.4	-0.7%
load-5	242.4	241.0	-0.6%
load-6	282.8	281.2	-0.6%

For each operational point the calculated torque obtained by the laser cut affected model is somewhat lower than the torque calculated with the unaffected model. As already mentioned the stator current input is identical for both modelling approaches. The lower calculated torque obtained with the affected model is the obvious implication of having a degraded magnetisation curve due to laser cutting as input for the affected modelling case. However the differences on the calculated torque are rather small (always smaller than 1%). In other words, the impact of laser cutting on the machine's torque is limited, which is related to

the limited impact of laser cutting on the magnetisation curve above 1.5T (see Fig. 2) and as we will see in Fig. 7a later on, the magnetic polarisation values for at least operational points load-2 to load-6 are indeed higher than 1.5T.

5.2 Calculated iron losses results

Based on the finite element computations for no-load and for the set of 70 load operational points over the entire torque versus speed range, the iron losses occurring in the stator yoke, stator teeth and rotor electrical steel parts are calculated using the approach described in section 3. Fig. 4 shows the results of all investigated operational points in terms of total iron losses (stator and rotor iron losses combined), obtained with the unaffected material model (Fig. 4a) and with the laser cut affected material model (Fig. 4b). In Fig. 5 the iron losses results shown in Fig. 4 are compared to each other. From this it can be concluded that including the laser cut effect into the machine modelling leads to a significant increase of the predicted iron losses of 25% up to 60%, but that the actual difference strongly depends on the specific operational point.

In order to better understand this dependence on the operational point of the total calculated losses (Fig. 4), and of the iron loss increase due to laser cutting (Fig. 5), an analysis is made of the peak magnetic polarisation occurring in the stator, as a function of the operational point. From Fig. 6, which shows histograms of the peak magnetic polarisation occurring in the stator for the no load operation, it can be concluded that the laser cutting effect shifts these magnetic polarisation amplitudes to slightly lower values. This is also linked with the limited but also deteriorating impact of laser cutting on the calculated torque, as already shown and discussed in Table 2. Also, it can be noticed that the characteristic magnetic polarisation of the stator teeth region is different than the one of the stator yoke region; this of course depends on the specific stator geometry of the investigated machine.

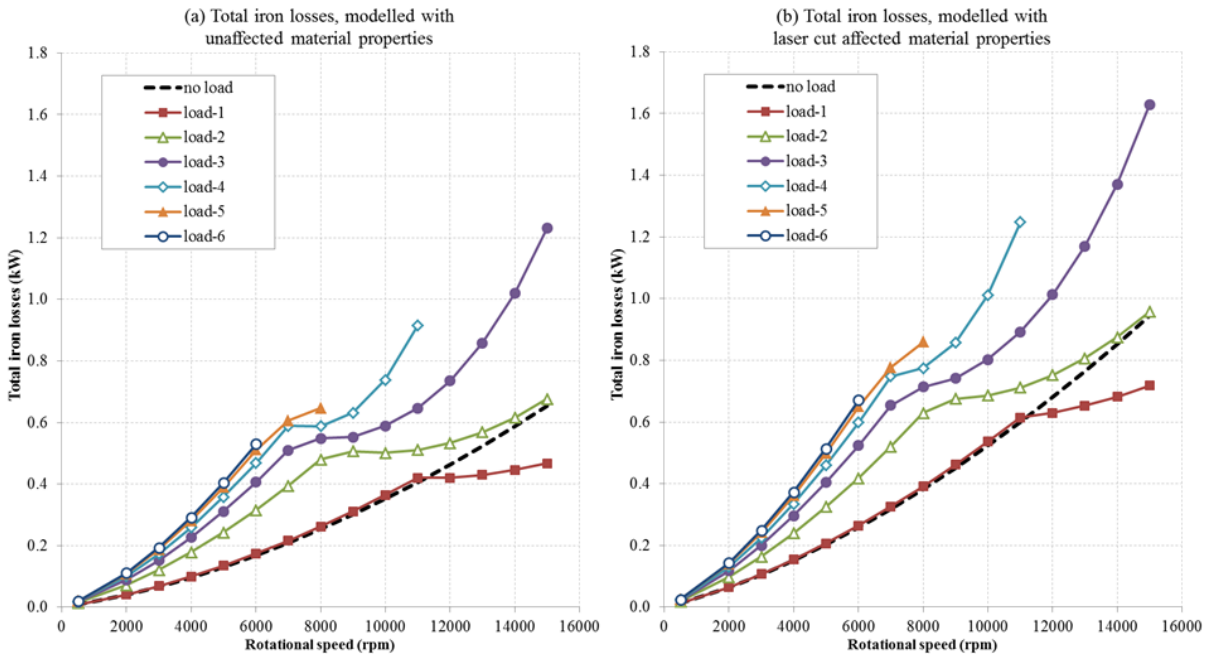

Figure 4: Total iron losses of stator and rotor combined, on the left hand side modelled with unaffected material properties (a) and on the right hand side modelled with laser cut affected material properties, for all considered no-load (dashed line) and load operational points over the entire speed range.

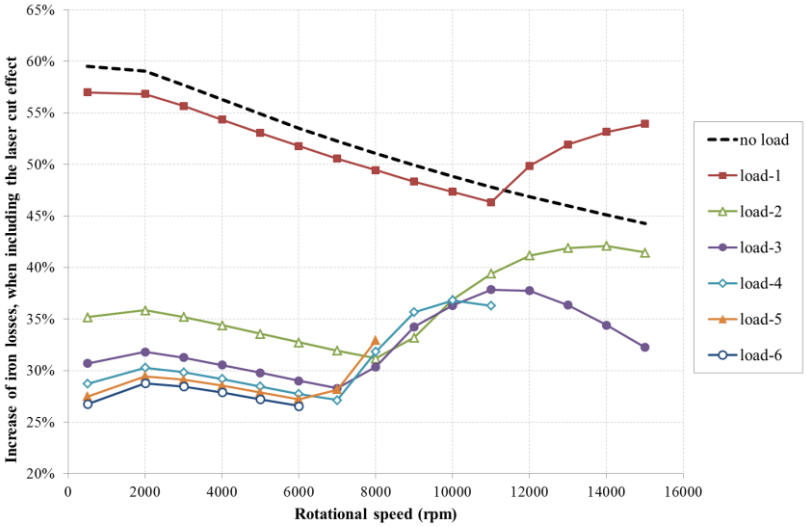

Figure 5: Comparison of the total iron losses obtained with the laser cut affected material model, versus the iron losses modelled with unaffected material properties, indicating the increase of predicted total iron losses when including the laser cut effect into the machine modelling.

In a further analysis of the magnetic polarisation values occurring at the stator, we focus on the laser cut affected case of the stator teeth region: Fig. 7a shows the dependence on the operational point of the characteristic magnetic polarisation amplitude of the stator teeth region (obtained as weighted average of the J-amplitude occurring in every stator teeth element, weighted over the surface area of these finite elements), evaluated for the laser cut affected case. For each load setting, two operational ranges as a function of rotational speed can be deduced, being the constant torque operation at low speeds (with constant magnetic flux), as well as the flux weakening operation at higher speeds.

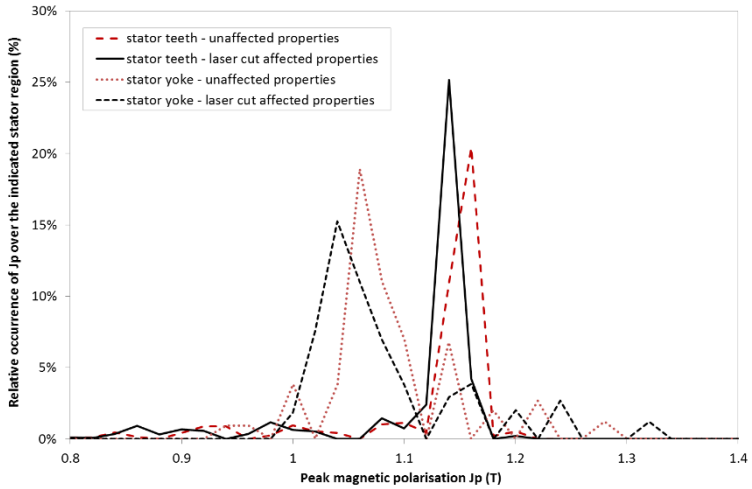

Figure 6: Histograms of the peak magnetic polarisation J_p occurring in the two stator sub-regions (stator teeth and stator yoke), at no load operation, and for both the affected and unaffected case. Histogram step size: $\Delta J_p = 0.02$T. When compared to the histograms of the unaffected case, the histograms of the affected case shift to slightly lower J_p.

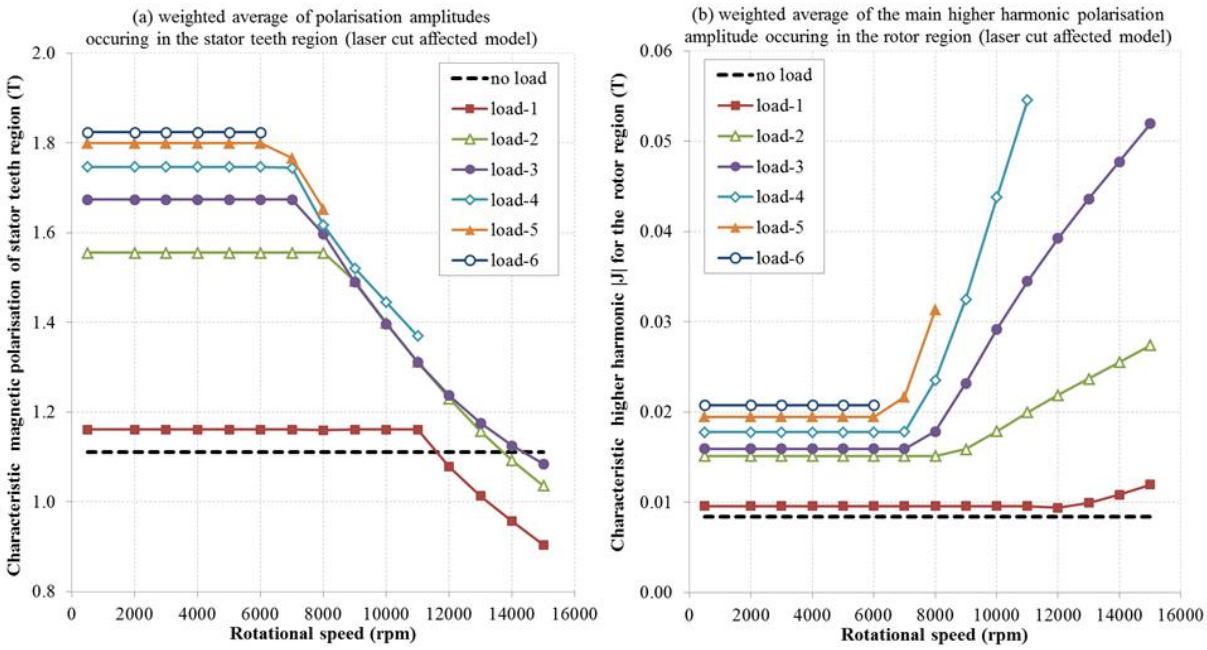

Figure 7: (a) Dependence on the operational point of the characteristic magnetic polarisation amplitude of the stator teeth region (obtained as weighted average of the J-amplitude occurring in every stator teeth element, weighted over the surface area of these finite elements), for the laser cut affected case. (b) Dependence on the operational point of the stator slotting main harmonic magnetic polarisation amplitude of the rotor region (obtained as weighted average of the harmonic amplitude occurring in every rotor element, weighted over their surface area), for the laser cut affected case.

The 'corner speed' between both operational ranges can also be noticed at the iron loss versus speed graphs of Fig. 4. Indeed, analysed for a certain load point, for speeds below this corner speed the magnetic flux distribution in the machine is identical (constant flux operation), and hence only the frequency (speed) has an impact on the iron losses. This frequency dependence is clearly visible for the no-load operational points having constant flux operation at all speeds (dashed line in Fig. 4).

Also, for increasing speeds the relative weight of the classical eddy current losses becomes more important in the total iron losses, which explains the decreasing tendency of the laser cut effect on the iron losses as a function of frequency (speed), which is clearly visible for the no-load situation in Fig. 5 (dashed line). Additionally, for the different load settings, such tendencies are also followed in case of the constant torque (constant flux) operation below the corner speed.

Within the constant flux operational area, the additional iron losses due to laser cutting relatively decrease for the higher torque operational points. This is because the magnetic flux levels in the machine are higher at higher torque, and at higher magnetic flux the relative impact on the losses due to laser cutting is lower, since only the magnetic domain wall motion is affected by it, and not the magnetic domain rotations occurring at higher magnetic flux.

This phenomenon also explains why at a given load operation the additional losses due to laser cutting start to increase again when the speed increases above the corner speed: indeed, in the flux weakening operation the magnetic flux level decreases and hence the relative laser cutting impact on the losses increases again.

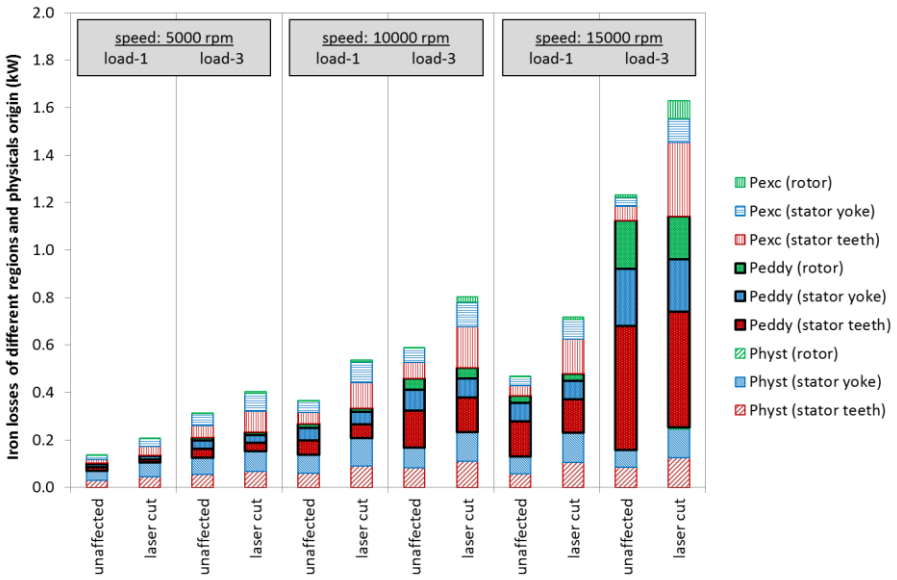

Figure 8: Iron loss separation into different components dealing with machine region and physical origin of the losses, for three different speeds and two different operational points. When comparing the affected case with the unaffected case, the increase of both hysteresis and excess losses is clear, whereas the classical eddy current losses are only indirectly impacted by the effect of the laser cutting on the magnetic flux level, which slightly decreases. When comparing load-3 to load-1 at 5000rpm, the differences in losses are explained by an increased magnetic flux level for load-3, whereas the harmonic content of the flux remains identical. For 10000 rpm and 15000 rpm, the differences in losses at load-1 and load-3 are explained by a combination of higher stator magnetic flux and higher harmonic content for the load-3 operational point when compared to load-1.

At the highest speeds and for high load operational points the total iron losses increase significantly as a function of speed, although the magnetic flux is further weakened. This is due to the increased higher harmonic content in both the stator and rotor magnetic flux waveforms, having a big impact on the classical eddy current losses. Indeed, the stator slotting harmonic becomes more important in the flux weakening operational range, due to the increase of the I_d stator current, to limit the inverter voltage within the flux weakening range. The harmonic content for each operational point in terms of load and speed can be evaluated in Fig. 7b, in which the J-amplitude of the main higher harmonic (being the 18th harmonic originating from the stator slotting) is visualised.

These additional classical eddy current losses due to the higher harmonic content can also be seen in Fig. 8, where a loss separation over the different regions and different physical origins is given. When comparing the load-3 to the load-1 operational point at 15000 rpm (so at identical fundamental frequency), a large increase of classical eddy current losses at the rotor is apparent, which is explained by roughly 5 times higher harmonic content for load-3 compared to load-1 at 15000 rpm (see Fig. 7b). Also the significant increase of classical eddy current losses at the stator teeth and yoke when going from load-1 to load-3 at this highest speed is explained to a large extent by also a higher harmonic content of the magnetic flux in the stator parts of the machine.

Moreover, since at high speeds and at high load operation, the classical eddy current losses due to the higher harmonic content of the magnetic flux become an important part of the total iron losses, the relative impact of laser cutting on the iron losses decreases again as function of speed, which can be seen in Fig. 5 for the load-3 operation at high speeds.

Nevertheless, it's important to stress out that for the operational points with the highest total iron losses (high load points within the flux weakening range), the amount of rotor losses is relatively higher than for the low loss operational points, which can become a critical issue thermally speaking in relation with the properties of the permanent magnets.

6 Comparison of modelled losses versus measured losses

6.1 Machine measurement methodology

After the comprehensive investigation of the machine, test bench measurements are done to validate the calculated losses. The test bench setup used in the measurements is shown in Fig. 9. Between the inverter and the e-machine is a box to measure the phase voltages and currents with a power analyser, as well as to enable no load and short circuit operation. The temperature of rotor and stator are measured with thermo-elements. All data is visualized and recorded in a test bench computer.

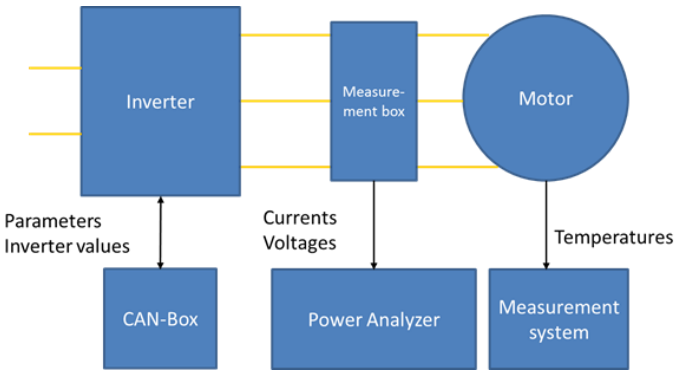

Figure 9: Schematic overview of the machine test bench setup

6.2 Comparison of modelled losses versus measured losses

With the set-up described in the section above, the measurements are done. The first test was the measurement of back-EMF and no-load losses. The no-load losses P_v consist of iron losses $P_{v,fe}$, magnet losses, bearing losses $P_{v,bearing}$ and air friction losses $P_{v,air}$. It is assumed that the magnet losses are much smaller in the no-load operation than the iron losses and are neglected. The iron losses are computed with equation (2), where the bearing and air friction losses are subtracted from the overall measured losses. The bearing losses are determined with a no-load test bench setup, whereas the air friction losses are based on CFD simulation results.

$$P_{v,fe} = P_v - P_{v,bearing} - P_{v,air} \tag{2}$$

The measured no-load iron losses at 5000, 10000 and 15000 rpm speeds are compared with the simulation results in Table 3. The results illustrate that the simulation enhancement by including the cutting effect on the magnetic properties is useful to fit the simulation better to the actual machine measurement. Especially the no load points at 10000 rpm and 15000 rpm show a good agreement between the computed iron losses with affected material properties and the machine measurement on the test bench. Only the 5000 rpm point is located between the simulation with unaffected material and those with affected material properties. It has to be pointed out however that at that operational point the measured torque is actually very low, and hence difficult to measure properly, when considering the measurement quality of the torque sensor in terms of tolerances into account, the measured iron losses at 5000 rpm have to be considered with a rather large error bar.

Table 3: No-load iron losses at three different speeds: comparison of the measured no-load iron losses, to the simulated no-load iron losses obtained by both models (unaffected material model and affected material model: laser cutting). For the simulated iron losses the absolute values in W are given, as well as their comparison to the measured losses (relative differences in %, between brackets).

Speed (rpm)	Measured iron losses (W)	Simulated iron losses (W); *unaffected material model*	Simulated iron losses (W); *affected material model*
5000	166	130 *(-22%)*	202 *(22%)*

10000	574	352 *(-39%)*	524 *(-9%)*
15000	925	655 *(-29%)*	944 *(2%)*

7 Conclusion

An improved methodology to compute the iron losses including the local magnetic degradation due to laser cutting is applied and validated on a PMSM traction machine, using an ArcelorMittal iCARe® electrical steel grade, developed specifically for automotive traction applications operating mainly at medium frequencies (400 Hz – 1kHz) and optimized for lowest iron losses to allow for extended drive ranges.

The additional iron losses due to laser cutting are of both hysteretic and excess loss nature. Machine calculations are carried out for both no-load and load operational points: the calculated torque values at iso-stator current are only slightly impacted by the cutting effect. The no-load iron losses calculations at higher speeds including the laser cut effect fit nicely with the measured iron losses, whereas the ordinary calculations with standard unaffected material properties significantly under-estimate the actually measured iron losses. In other words including the cutting effect into the modelling makes it possible to improve the overall accuracy of the total loss prediction, which enables more accurate design of such applications.

For the load operational points, the iron losses increase with 25% to 60% when incorporating the laser cut effect into the modelling. The dependence of these additional losses on the speed and load operation is related to the magnetic polarisation amplitude occurring in the stator and to the harmonic content of the magnetic polarisation waveform in both stator and rotor components.

References

[1] S. Luthardt, S. Schmitz, A. Heitmann, D. Gerling, *"Improved electric drive analysis methodology for electrical vehicle propulsion",* Proceedings of the European Power Electronics Conference, EPE'16 (ECCE Europe), 2016.

[2] G. Bertotti, *"General properties of power losses in soft ferromagnetic materials",* IEEE Trans. Magn. 24(1), pp. 621-630 (1988).

[3] A. Boglietti, A. Cavagnino, M. Lazzari, M. Pastorelli, *"Predicting iron losses in soft magnetic materials with arbitrary voltage supply: an engineering approach",* IEEE Trans. Magn. 39(2), pp 981-989 (2003).

[4] L. Vandenbossche, S. Jacobs, E. Attrazic, *"Motor performance improvement via ArcelorMittal's iCARe® electrical steel range for automotive applications",* Proceedings of EVS-28 conference, 2015, Seoul.

[5] L. Vandenbossche, S. Jacobs, F. Henrotte, *"Impact of cut edges on magnetisation curves and iron losses in e-machines for automotive traction",* World Electric Vehicle Journal, Vol.4, ISSN 2032-6653, WEVA (2010), pp. 587-596. Proceedings of EVS-25 conference, 2010, Shenzhen.

[6] J. Rens, S. Jacobs, L. Vandenbossche, E. Attrazic, *"Effect of stator segmentation and manufacturing degradation on the performance of IPM machines, using iCARe electrical steels",* Proceedings of EVS-29 conference, 2016, Montréal.

[7] S. Elfgen, S. Steentjes, S. Böhmer, D. Franck, K. Hameyer, *"Influences of material degradation due to laser cutting on the operating behaviour of PMSM using a continuous material model",* IEEE Trans. Industry Applications, 53(3), pp. 1978-1984 (2017).

[8] R. Siebert, A. Wetzig, E. Beyer, B. Betz, C. Gruenzweig, E. Lehmann, *"Localized investigation of magnetic bulk property deterioration of electrical steel",* IEEE Xplore Conference proceedings of the Electric Drives Production Conference, EDPC 2013 (Nürnberg), pp. 60-64.

[9] R. Siebert, J. Schneider, E. Beyer, *"Laser Cutting and Mechanical Cutting of Electrical Steels and its Effect on the Magnetic Properties"*, IEEE Trans. Magn., Vol. 50(4), 2001904, pp. 1-4 (2014.

Authors

Lode Vandenbossche is research engineer at ArcelorMittal Global R&D. Based in Gent, Belgium, his research topics are electrical steels and electromagnetic applications, with emphasis on advanced magnetic characterisations, magnetic material modelling and the impact of machine production processes. He obtained a MSc degree in electromechanical engineering and a PhD degree at Ghent University about the link between magnetic properties and the microstructure of steels.

Sven Luthardt was born in 1989 in Sonneberg, Germany. He received the M.S degree in electrical engineering from the University of Erlangen-Nürnberg in 2013. He is currently working towards the Ph.D. degree at Porsche AG, Weissach, Germany in cooperation with the Universität der Bundeswehr München, Neubiberg, Germany. His research interests include the loss analysis of electrical machines for electric vehicle propulsion and the investigation of inverter effects in e-machine simulation process.

Sigrid Jacobs graduated in electro-technical engineering at Ghent University and obtained an MBA at the Vlerick School for management, Belgium. After developing electrical steels at the metallurgy lab of the Ghent university, she joined the ArcelorMittal group and was involved in engineering projects. Now she is portfolio director of the group's R&D activities in Electrical Steels.

Stefan Schmitz was born in 1979 in Waiblingen, Germany. He received the diploma and Ph.D. degrees in electrical engineering from University of Stuttgart in 2005 and 2010, respectively. In 2010, he joined AMK Arnold Müller GmbH & Co. KG, Kircheim, Germany as project manager. In 2011, he was with Porsche Engineering Services GmbH, Bietigheim-Bissingen, as development engineer. Since 2012, he has been with Dr. Ing. h.c. F. Porsche AG, Weissach, Germany, as advanced engineering specialist within the advanced engineering drivetrain and electric drives department.

Emmanuel Attrazic is a superior environment technician. After acquiring production experience in the electrical steel production site of St-Chély d'Apcher (ArcelorMittal), he joined the plant's metallurgy-quality lab. He further specialised in mechanical and magnetic measurements, beyond the needs of routine production.

Axel Heitmann was born in 1968 in Erlangen, Germany. He received the diploma and Ph.D. degrees in mechanical engineering from the Technical University of Munich in 1993 and 1998, respectively. In 1999, he joined ZF Friedrichshafen AG, Friedrichshafen, Germany, as advanced engineering specialist. From 2004 to 2012, he was with Audi AG, Ingolstadt, Germany, as advanced engineering specialist and project manager. Since 2013, he has been with Dr. Ing. h.c. F. Porsche AG, Weissach, Germany, as manager advanced engineering drivetrain and electric drives.